Electrical characterization and extraction of activation energies of the defect states in the LaAlO3/SrTiO3 heterostructure

Yoann Lechaux, Yu Chen, Albert Minj, Florencio Sánchez, Gervasi Herranz, Laurence Méchin, Bruno Guillet

Electrical characterization and extraction of activation energies of the defect states in the $LaAlO_3/SrTiO_3$ heterostructure

Yoann Lechaux[1,a)], Yu Chen[2], Albert Minj[3], Florencio Sánchez[2], Gervasi Herranz[2], Laurence Méchin[1] and Bruno Guillet[1]

[1]Normandie Univ, UNICAEN, ENSICAEN, CNRS, GREYC, 14000 Caen, France
[2]Institut de Ciència de Materials de Barcelona (ICMAB-CSIC), Campus UAB, 08193 Bellaterra, Catalonia, Spain
[3]IMEC, Kapeldreef 75, Leuven 3000, Belgium

[a)]Author to whom correspondence should be addressed: yoann.lechaux@unicaen.fr.

Abstract

In this work, we study the electronic properties of defects in the $LaAlO_3/SrTiO_3$ heterostructure, which is known to host a high mobility two-dimensional electron gas (2DEG) at the interface. This 2DEG also shows photoconductance, which could be related to defects that act as deep centers trapping and releasing carriers by interaction with light. This phenomenon has raised an interest for the identification of deep energy levels in the $LaAlO_3/SrTiO_3$ heterostructure. We have studied the defect state properties using electrical characterization such as capacitance-voltage (C-V), current-voltage (I-V) measurements and Deep-Level Transient Fourier Spectroscopy (DLTFS). From C-V and I-V analysis, a hysteresis was observed indicating an effect of mobile charges in the $LaAlO_3$. Using DLTFS we identify three defect states located at around 0.17 eV below conduction band and at 0.23 eV and 0.26 eV above the valence band. These defect states were attributed to defects in $SrTiO_3$ such as strontium vacancies or titanium vacancies. We identify a fourth defect state having an energy of about 0.69 eV below the conduction band that could be related to oxygen vacancies in $LaAlO_3$ or in $SrTiO_3$. In addition, the observation of an effect of the electric field with DLTFS indicated that oxygen vacancies might be involved in Fowler-Nordheim or trap-assisted tunneling through the $LaAlO_3$ the layer.

Oxide-based peroskite heterostructures show a wide range of physical properties[1] such as ferroelectricity,[2,3] superconductivity[4–6] or ferromagnetism,[7,8] which make them appealing for the development of multifunctional materials for a wide range of applications[9–12]. One particularly interesting example is that of $LaAlO_3/SrTiO_3$ heterostructures which host two-dimensional electron gase (2DEG)[6] with strong Rashba spin-orbit coupling[13,14] and large spin-to-charge conversion,[15] as well as two-dimensional superconductivity, with transition temperature around 300 mK[16,17]. Other applications include their use as channel materials in transistors[12,18] or exploit the tunability of the 2DEG by electrostatic gating,[16,17,19–21] or by light as in persistent photoconductance[22–25]. In this regard, we have demonstrated recently that the carrier population of the $LaAlO_3/SrTiO_3$ interface can be increased or depleted using light pulses with different wavelengths,[22] a property which could be potentially useful to mimic spike-timing-dependent plasticity using the 2DEG as artificial synapses stimulated by optical pulses with duration down to microsecond.[9] We proposed that this unusual photoconductance could be explained by the presence of defects in the $LaAlO_3/SrTiO_3$ heterostructure, particularly to the so-called DX-centers,[26] which would act as trapping centers that capture and release carriers by interacting with light.[22] Furthermore, a longstanding question is the charge density inferred from Hall measurements, which is about one order of magnitude smaller than the value expected from the polar discontinuity model.[27–30] Related to this issue, it has been proposed that polar discontinuity triggers the spontaneous formation of some defects[31] that could be trapping centers in the $LaAlO_3/SrTiO_3$ heterostructure related to point defects[32] which would induce electron accumulation at the interface[33] with a depth of few nanometers.[34] Moreover, the characterization of defect states is a central piece of research for applications of semiconductors in electronic devices.[35]

These observations raise the interest of identifying trapping centers in the $LaAlO_3/SrTiO_3$ heterostructure. Several works have reported defect state properties in $LaAlO_3$[36–38] or in $SrTiO_3$.[39–41] Regarding bulk $LaAlO_3$, some studies from K. Xiong *et al.* have been performed to estimate the energies of the defect states using the density functional theory (DFT).[36,37] Their calculations showed that oxygen interstitial states such as I_O^- lie at about 0.5 eV above the valence band while I_O^{-2} lie in the valence band. Moreover, they calculated the energy of the oxygen vacancy states, such as V_O^0 to be about 0.8 eV below conduction band while V_O^+ and V_O^{+2} states lie at about 0.6 eV and 0.55 eV, respectively, below the conduction band. In the context of $LaAlO_3/SrTiO_3$ interfaces, L. Yu *et al.*[32] reported on different defect states, including Ti_{Al} antisites in the $LaAlO_3$ layer, Al_{Ti} antisites at the interface and oxygen vacancies at the surface of $LaAlO_3$ that may cause the 2DEG.[31] Moreover, oxygen vacancies in the $LaAlO_3/SrTiO_3$ heterostructure were studied using density functional theory[42,43] and were experimentally related to the enhancement of electrical conductivity.[44]

Regarding $SrTiO_3$, A. K. Ghosh *et al.* evidenced four defect states from 0.26 eV to 0.43 eV above valence band[39] by thermally stimulated current method. Using the same technique, B. Wang *et al.* found five energies from 0.15 eV to 0.86 eV.[41] Osawa *et al*. reported an activation energy of about 0.06 eV above valence band for strontium vacancies.[45] Y. Seo *et al.* made DLTS measurement to characterize Cr-$SrTiO_3$ on silicium substrate but all the identified traps were related to silicium.[46] F. A. Selim *et al.* used the positron annihilation lifetime spectroscopy to find the defect lifetimes in $SrTiO_3$[47] (however, this technique cannot give the defect state energies). On the other hand, T. Tanaka *et al.* calculated defect states energies from 0.11 eV to 0.20 eV above valence band for strontium vacancies, from 0.26 eV to 0.84 eV above valence band for titanium vacancies and from 0.08 eV to 0.21 eV below conduction band for oxygen vacancies.[48] A. Janoti *et al*. calculated the defect states in the *n*-doped $SrTiO_3$ and they found energies of about 0.51 eV below conduction for oxygen vacancies (V_0^+), from 0.20 eV to 0.30 eV above valence band for strontium vacancies and from 0.58 eV to 0.81 eV above valence band for titanium vacancies depending on charge state.[49] Besides, D. Manger *et al.* reported oxygen vacancy energies from 0.8 eV to 1.2 eV below conduction band in the $SrTiO_3$ films grown by atomic layer deposition.[50] B Liu *et al.* calculated the energies for interstitial defect states in $SrTiO_3$ and showed a large variety of defect states.[51]

As pointed out above, defect formation and detection has been studied in $LaAlO_3/SrTiO_3$ heterostructures. A few experimental works have reported on defect state properties in the $LaAlO_3/SrTiO_3$ heterostructure, yet some fundamental aspects, such as their activation energy, have not been identified. For example, A. Kalabukhov *et al.* observed the impact of oxygen vacancies on the electrical properties using cathode and photoluminescence techniques.[52] N. Palina *et al.* showed oxygen orbital states using X-ray spectroscopies,[44] A. Gloter *et al.* observed the distribution of point defects at the interface using scanning transmission electron microscopy[53] and G. Yuan *et al.* reported on the behavior of oxygen vacancies at the $LaAlO_3/SrTiO_3$ heterostrucutre using positron annihilation spectroscopy.[54] In our work we extracted defect properties that cannot be accessed using these methods, such as the activation energies and capture cross-sections of the defect states using Deep-Level Transient Fourier Spectroscopy (DLTFS).[55,56]

All the measurements were performed on a isolated capacitor device based on the $LaAlO_3/SrTiO_3$ heterostructure, which was fabricated through a sequential deposition process combined with photolithography. First of all, pulsed laser deposition (PLD) was exploited to deposit an amorphous ~60 nm thick $LaAlO_3$ layer at room temperature on substrate $SrTiO_3$ with annular geometry defined by photolithography and lift-off. Afterward, an epitaxial $LaAlO_3$ layer with thickness of 12 unit cell (around 4.6 nm) was grown on the annularly patterned $SrTiO_3$ using PLD at 650°C and oxygen partial

pressure about 10^{-4} mbar. At the end of the deposition, we cooled down the sample in the oxygen rich atmosphere to minimize the formation of oxygen vacancies. Subsequently, the photolithography was carried out again to define top electrodes position on the center of the annulars, followed by the gold top contact deposition using evaporation and lift-off. Thus, a capacitor structure is formed ($Au/LaAlO_3/SrTiO_3$) where the 2DEG at the $LaAlO_3/SrTiO_3$ interface, used as bottom electrode, was contacted by ultrasonic aluminium wire-bonding. FIG. 1 shows the heterostructure and the measurement sketch (FIG. 1(a)) and a top view of the circular devices (FIG. 1(b)) among which the 800 µm diameter size capacitor was measured. Details on the setup description and on the method for the Deep-Level Transient Fourier Spectroscopy analysis can be seen in supplementary material.

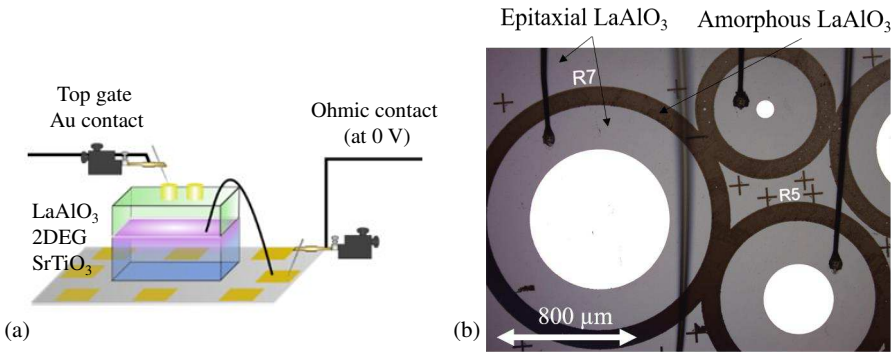

FIG. 1. (a) Schematics of the $LaAlO_3/SrTiO_3$ heterostructure showing a 2DEG at the interface (in purple color) and (b) a top view of the fabricated circular devices.

The capacitance-voltage (*C*-*V*) and the current-voltage (*I*-*V*) characteristics were measured at room temperature with an AC signal at 1 MHz. Two voltage sweeps in opposite directions, from positive to negative values (1) and from negative to positive values (2), were performed one after the other to observe the impact of the defect states on the static characteristics, such as hysteresis effects.

Condidering an *n*-type 2DEG at the $LaAlO_3/SrTiO_3$ interface, the heterostructure would behave as a *p*-metal-oxide-semiconductor (MOS) capacitor. At high frequency, the capacitance generally increases with the positive voltage from the depletion regime to the accumulation regime. FIG. 2(a) shows the capacitances from parallel (FIG. 2(c)) and series (FIG. 2(d)) *RC* models as a function of the voltage at room temperature. A large difference between both capacitances was observed. Contrary to the parallel capacitance C_P, the series capacitance C_S is increasing with the voltage from about 12 pF at -5 V to about 68 pF at 1 V. This trend indicates that the series *RC* model might be more relevant,

although no saturation of the series capacitance was observed for the range of analyzed voltages. However, in these models, the capacitance is drastically reduced at high frequency (> 10 kHz) as mentioned in previous works.[57–59] Conversely, S.K. Kim *et al.*[57] proposed two different models for the depletion and accumulation regimes. In accumulation, the model is a series combination of a resistance and a parallel *RC* circuit (FIG. 2(e)). The series resistance R_S comes from the 2DEG in the $SrTiO_3$ and the parallel *RC* circuit corresponds to the $LaAlO_3$ layer. In depletion, the model becomes more complex and it is a series combination of the 2DEG resistance and two parallel *RC* circuits corresponding to the $SrTiO_3$ and to the $LaAlO_3$ layers.

However, a few observations can be made from the *C-V* characteristics in FIG. 2(a). Even though the dielectric constant for $LaAlO_3$ cannot be extracted reliably, we can clearly observe the two regimes. More specifically, accumulation of the *n*-2DEG is observed for voltages above -1 V, while its depletion, associated with the reduction of C_S, is seen for voltages below -1 V, up to a saturation for complete depletion. Besides, a hysteresis is observed for voltages between 0.5 V to -3.5 V with a maximum difference of about 0.45 V between the two sweep at C_S = 40 pF. This voltage shift may hint towards charge transfer through defects under the influence of electric field, and such charged defects could be possibly linked to oxygen vacancies in $LaAlO_3$.[60] S.K. Kim *et al.* and C.W. Bark *et al.* related this phenomenon to an electric-field induced redistribution of the oxygen vacancies in the $LaAlO_3$ up to the interface which leads to a switchable hysteretic response[61,62] as observed on the I-V characteristics.

FIG. 2(b) shows the *I-V* characteristics at room temperature. We observed different behaviors between the two voltage sweep directions, mainly for negative gate voltages. For sweep (1) and for voltages between 1.5 V and 0 V, the current is decreasing while the voltage decreases. Then, in the bias range between 0 V and -5 V, the current initially increases with the applied negative bias up to -2.5 V and decreases until -5 V forming a hump in the *I-V* characteristics as reported by S.K. Kim *et al.*.[62] This observed hump indicates a sudden increase of the resistance for biases below -2.5 V. Then for sweep (2) from -5 V to 1.5 V, no hump is observed and the current level starts at the same level as that for the previous sweep. Similar features in *I-V* curve were previously observed and were attributed to oxygen vacancy drift[60] and might be related to the hysteresis observed in the *C-V* curve. This hump on the *I-V* curve must be associated to a drop in current due to full depletion of the *n*-2DEG which induced an increase of the resistance beneath of the electrode.

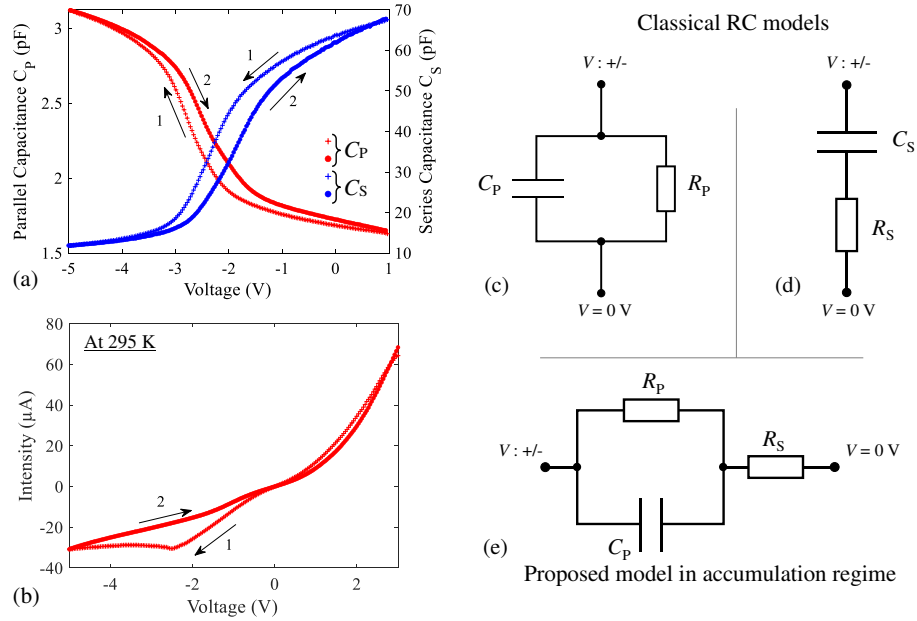

FIG. 2. (a) Capacitance-voltage and (b) current-voltage characteristics for two different voltage sweep directions, at room temperature. Different *RC* models : (c) parallel circuit, (d) series circuit and (e) the combination of a parallel and series circuits.

In order to evaluate the defect state properties, DLTFS measurements were performed for various time windows t_w. Fig. 3 shows the DLTFS spectra for t_w = 49 ms, 146 ms, 293 ms, 586 ms, 977 ms while U_R = -0.8 V, U_P = -3.0 V and t_P = 1.0 s. We observed two main different regions in the spectra, namely, one for temperatures below 150 K and another for temperatures above 300 K. For temperatures below 150 K, we found three significant peaks, one positive (T_1) and two negative peaks (T_2 and T_3), see Fig. 3(a). For temperatures above 300 K, a significant positive peak (T_4) was observed, see Fig. 3(b). We noticed an increase of T_2, T_3 and T_4 amplitudes with increasing t_w. In contrast, the T_1 amplitude decreases when t_w increases, which indicates a much lower relaxation time for T_1 in comparison to T_2, T_3 and T_4.[55] Besides, the temperatures of the DLTFS peaks shift toward lower values with increasing t_w, what is in agreement with a decrease of the emission rate. From the Arrhenius diagram (Fig. 3(c)), we first extracted the activation energy E_T. For the analysis we considered that the $LaAlO_3$ and $SrTiO_3$ are n-type majority materials. The different extracted energies are about 0.17 ± 0.03 eV below conduction band for T_1, 0.23 ± 0.03 eV above valence band for T_2, 0.26 ± 0.06

eV above valence band for T_3 and 0.69 ± 0.03 eV below conduction band for T_4. T_1, T_2 and T_3 show shallow energy levels comparable to the ones observed in $SrTiO_3$[39,41,45,48,49] while T_4 shows a deeper energy level. Then we extracted the capture cross-section σ_T using mean effective masses (0.4 for electrons and 1.2 for holes)[63] for the heterostructure. Values of about $7 \cdot 10^{-15}$ cm^2, $2 \cdot 10^{-15}$ cm^2, $5 \cdot 10^{-14}$ cm^2, and $7 \cdot 10^{-19}$ cm^2 were found for T_1, T_2, T_3 and T_4 respectively. Although not exact, these values give an order of magnitude of the capture cross-section.

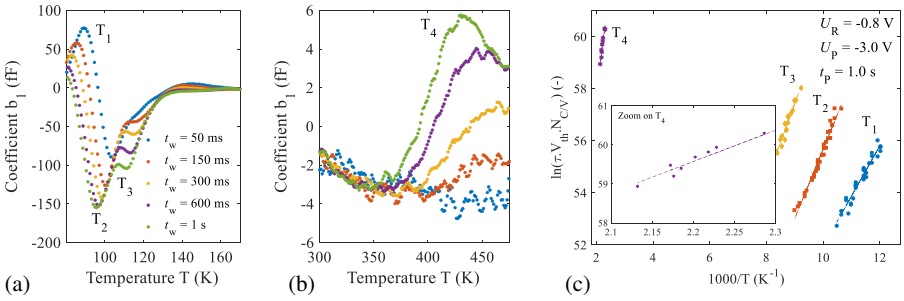

Fig. 3. DLTFS spectra of the $LaAlO_3/SrTiO_3$ heterostructure for various time windows t_w and for U_R = -0.8 V, U_P = -3.0 V and t_P = 1.0 s, at (a) low and (b) high temperature regions. (c) The Arrehnius diagram extracted for all the defect states.

To determine the origin of the observed defect states in the $LaAlO_3/SrTiO_3$ heterostructure, DLTFS measurements were carried out for various reverse and pulse voltages while keeping other parameters constant. These two variations allow, for example, to distinguish interface and bulk traps.[64,65] In the following, we focus on the study of the T_4 trap center at high temperature ~~which, as we argue below, might be related to oxygen vacancies in the $LaAlO_3$ layer~~. A similar analysis for the T_1, T_2 and T_3 traps is more complicated, due to the overlap of the corresponding peaks.

Fig. 4(a) shows the DLTFS spectra for reverse voltages U_R from -0.4 V to -1.0 V, keeping other parameters fixed at U_P = -3.0 V, t_P = 1 s and t_w = 977 ms. The data indicate an increase of the T_4 peak amplitude and a shift to lower temperatures when the reverse bias is changed from -0.4 V to -1.0 V. These both observations indicate that the trap states associated with the T_4 peak cannot be related to band-like defect states at the interface between $LaAlO_3$ and $SrTiO_3$, otherwise a decrease of the peak amplitude should be observed. On the other hand, an increase of the reverse bias from -0.4 V to -1.0 V should enhance the upward band bending close to the interface at the $SrTiO_3$ side (Fig. 4(c)). This would be accompanied by a narrowing of the 2DEG and a lowering of the trapped electron density at the interface associated to the bulk oxygen vacancies in the $SrTiO_3$, which should manifest as a

decrease of the DLTFS amplitude. However, this contradicts the increase of the peak amplitude with U_R observed in the DLTFS spectra in Fig. 4(a). We therefore conclude that the T_4 peak might not be related to bulk oxygen vacancies in $SrTiO_3$.

To explain the experimental data, we can invoke other phenomena based on trap assisted tunneling, Folwer-Nordheim tunneling or Poole-Frenkel effect. Indeed, an increase of the reverse bias from -0.4 V to -1.0 V should induce an increase of the electric field in the $LaAlO_3$ layer. In turn, this would be associated with a lowering of the effective barrier thickness between the oxygen vacancy levels located within the $LaAlO_3$ layer or in the bulk $SrTiO_3$ and the Au gate contact. For high negative pulse voltages, the levels of oxygen vacancies in both $SrTiO_3$ and $LaAlO_3$ are below the Au Fermi level. Thus, electrons can be transfered from the gate contact to the $LaAlO_3$ oxygen vacancies (Fig. 4(c)) by trap assisted tunneling, as similarly reported by K. Song *et al.* in their recent experimental work[66]. Moreover, these electrons can also be transferred up to $SrTiO_3$ oxygen vacancies by Fowler-Nordheim tunneling. As the effective barrier thickness diminishes when the voltages goes toward -1.0 V, a higher trapped electron density will result in an increase of the DLTFS peak amplitude. Therefore, the variation of the T_4 peak with U_R would be in agreement with the assumption of either trap assisted tunneling or with Fowler-Nordheim tunneling through $LaAlO_3$.

In order to validate this assumption, DLTFS measurements were carried out for various pulse voltages U_P between -1 V to -3.5 V at U_R = -0.95 V, t_P = 1 s and t_w = 977 ms (Fig. 4(b)) to maximise the DLTFS signal. No shift is observed when changing U_P = -1 V to U_P = -3.5 V indicating that the emission rate is quasi constant, so the T_4 peak might be related to bulk traps, thus supporting the view that the T_4 peak should be related to defects spread over the $SrTiO_3$ or $LaAlO_3$ layers. Note that in the case of band-like states, an increase of the pulse voltage would induce a shift of the DLTFS peak accompanied by an increase of its amplitude. As no shift is observed, it means that the traps are not just located at the interface but distributed across the $SrTiO_3$ or the $LaAlO_3$ layers. Besides, we found an increase of the DLTFS peak amplitude with the increase of pulse voltage from -1.0 V to -3.5 V which is related to the increase of trapped charge density. This observation is consistent with the adscription of tunnel effects through $LaAlO_3$, although it is difficult to distinguish whether the T_4 peak is related to oxygen vacancies in the $LaAlO_3$ layer or in the $SrTiO_3$ substrate.

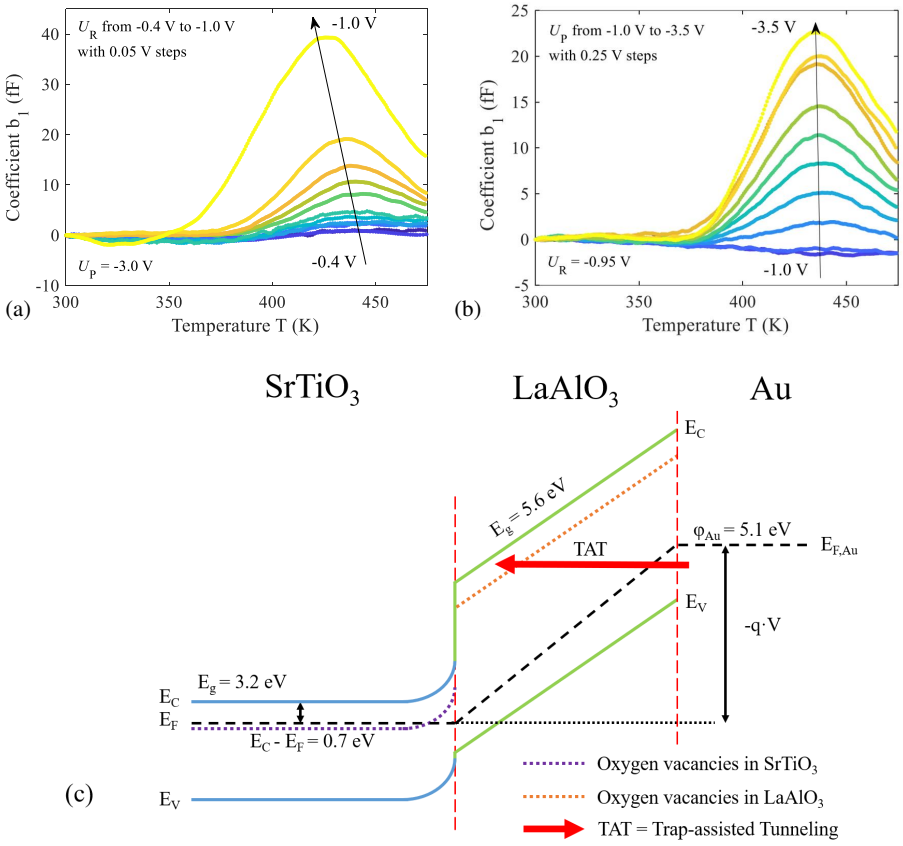

Fig. 4. (a) DLTFS spectra of the $LaAlO_3$/ $SrTiO_3$ heterostructure for various reverse voltages U_R from -0.4 V to -1 V, keeping fixed U_P = -3.0 V, t_P = 1.0 s and t_w = 977 ms. (b) DLTFS spectra for various pulse voltages U_P from -1 V to -3.5 V at U_R = -0.95 V, t_P = 1.0 s and at t_w = 977 ms. (c) Schematic of the band diagram of the Au/$LaAlO_3$/$SrTiO_3$ heterostructure for a gate voltage of -3.0 V.

After analysing the T_4 peak, we now turn the discussion of the other peaks observed in the DLTFS spectra. Comparing the extracted activation energies in the previous literature[48,49,51] with our observations, the T_1 peak energy close to the conduction band could be associated to interstitial titanium defect I_{Ti} in its neutral state. T_2 and T_3 peaks might be related to defect states in the $SrTiO_3$ such as strontium vacancies V_{Sr} or antisites Ti_{Sr}. Also, the extracted energy levels for T_2 to T_3 close to the valence band, lower than 0.3 eV, could not be related to titanium vacancies V_{Ti} as it shows deeper energy-level.

In summary, we studied the defect state properties of the in a $LaAlO_3/SrTiO_3$ heterostructure. We detected four defect states and their energies and capture cross sections were extracted. Three defect states were attributed to $SrTiO_3$ showing shallow energy levels at 0.17 eV below the conduction band and from 0.23 eV to 0.26 eV above the $SrTiO_3$ valence band. A fourth defect was attributed to oxygen vacancies in the $SrTiO_3$ or $LaAlO_3$ layers with an energy of about 0.69 eV below the conduction band. More importantly, we demonstrated the DLTFS can be a reliable method, showing similar results in comparison to other experimental techniques. With this in view, we propose that DLTFS could provide useful insights into some problems that are still under debate. For instance, it is kown that carrier densities at the $LaAlO_3/SrTiO_3$ interface are significantly lower than the ones expected from the polar catastrophe model[4], while larger values are observed at some $RTiO_3/SrTiO_3$ (R = rare earth) interfaces[67]. In this regard, DLTFS could provide a means to explore whether the reduction of trapping centres could be correlated with the transport properties of those interfaces.

Supplementary material

See supplementary material for the setup description and the method for the Deep-Level Transient Fourier Spectroscopy analysis.

Acknowledgments

We acknowledge financial support from Spanish Ministry of Science and Innovation (MCIN/AEI/10.13039/501100011033) through the Severo Ochoa FUNFUTURE (CEX2019-000917-S) and Grants No. PID2020-118479RB-I00 and PID2020-112548RB-I00, and by European Regional Development Fund "A way of making Europe".

Data availability

The processed data required to reproduce these findings cannot be shared at this time as the data also forms part of an ongoing study.

References

[1] J. Heber, Nature **459**, 28 (2009).

[2] D.J.R. Appleby, N.K. Ponon, K.S.K. Kwa, B. Zou, P.K. Petrov, T. Wang, N.M. Alford, and A. O'Neill, Nano Lett. **14**, 3864 (2014).

[3] T. Mikolajick, U. Schroeder, and S. Slesazeck, 2018 Int. Symp. VLSI Technol. Syst. Appl. VLSI-TSA 2018 1 (2018).

[4] S. Thiel, G. Hammerl, A. Schmehl, C.W. Schneider, and J. Mannhart, Science (80-.). **313**, 1942 (2006).

[5] G. Herranz, M. Basletić, M. Bibes, C. Carrétéro, E. Tafra, E. Jacquet, K. Bouzehouane, C. Deranlot, A. Hamzić, J.M. Broto, A. Barthélémy, and A. Fert, Phys. Rev. Lett. **98**, 3 (2007).

[6] A. Ohtomo and H.Y. Hwang, Nature **427**, 423 (2004).

[7] A. Urushibara, Y. Moritomo, T. Arima, A. Asamitsu, G. Kido, and Y. Tokura, Phys. Rev. B **51**, 14103 (1995).

[8] J. Nassar, M. Viret, M. Drouet, J.P. Contour, C. Fermon, and A. Fert, MRS Proc. **494**, 231 (1997).

[9] Y. Chen, B. Casals, F. Sánchez, and G. Herranz, ACS Appl. Electron. Mater. **1**, 1189 (2019).

[10] J. Varignon, L. Vila, A. Barthélémy, and M. Bibes, Nat. Phys. **14**, 322 (2018).

[11] Y. Lei, Y. Li, Y.Z. Chen, Y.W. Xie, Y.S. Chen, S.H. Wang, J. Wang, B.G. Shen, N. Pryds, H.Y. Hwang, and J.R. Sun, Nat. Commun. **5**, 1 (2014).

[12] N. Reyren, M. Bibes, E. Lesne, J.M. George, C. Deranlot, S. Collin, A. Barthélémy, and H. Jaffrès, Phys. Rev. Lett. **108**, 1 (2012).

[13] D. Stornaiuolo, C. Cantoni, G.M. De Luca, R. Di Capua, E. Di Gennaro, G. Ghiringhelli, B. Jouault, D. Marrè, D. Massarotti, F.M. Granozio, I. Pallecchi, C. Piamonteze, S. Rusponi, F. Tafuri, and M. Salluzzo, Nat. Mater. **15**, 278 (2016).

[14] G. Herranz, G. Singh, N. Bergeal, A. Jouan, J. Lesueur, J. Gázquez, M. Varela, M. Scigaj, N. Dix, F. Sánchez, and J. Fontcuberta, Nat. Commun. **6**, 1 (2015).

[15] D.C. Vaz, P. Noël, A. Johansson, B. Göbel, F.Y. Bruno, G. Singh, S. McKeown-Walker, F. Trier, L.M. Vicente-Arche, A. Sander, S. Valencia, P. Bruneel, M. Vivek, M. Gabay, N. Bergeal, F. Baumberger, H. Okuno, A. Barthélémy, A. Fert, L. Vila, I. Mertig, J.P. Attané, and M. Bibes, Nat. Mater. **18**, 1187 (2019).

[16] A.D. Caviglia, S. Gariglio, N. Reyren, D. Jaccard, T. Schneider, M. Gabay, S. Thiel, G. Hammerl, J. Mannhart, and J.M. Triscone, Nature **456**, 624 (2008).

[17] G. Singh, A. Jouan, G. Herranz, M. Scigaj, F. Sánchez, L. Benfatto, S. Caprara, M. Grilli, G. Saiz, F. Couëdo, C. Feuillet-Palma, J. Lesueur, and N. Bergeal, Nat. Mater. **18**, 948 (2019).

[18] X.B. Lu, H.B. Lu, Z.H. Chen, X. Zhang, R. Huang, H.W. Zhou, X.P. Wang, B.Y. Nguyen, C.Z.

Wang, W.F. Xiang, M. He, and B.L. Cheng, Appl. Phys. Lett. **85**, 3543 (2004).

[19] D. V. Christensen, F. Trier, Y.Z. Chen, A. Smith, J. Nygård, and N. Pryds, Appl. Phys. Lett. **102**, 1 (2013).

[20] W. Dai, S. Adhikari, A.C. Garcia-Castro, A.H. Romero, H. Lee, J.W. Lee, S. Ryu, C.B. Eom, and C. Cen, Nano Lett. **16**, 2739 (2016).

[21] H. Guo, W.A. Saidi, and J. Zhao, Phys. Chem. Chem. Phys. **18**, 28474 (2016).

[22] Y. Chen, Y. Lechaux, B. Casals, B. Guillet, A. Minj, J. Gázquez, L. Méchin, and G. Herranz, Phys. Rev. Lett. **124**, 246804 (2020).

[23] Y. Chen, B. Casals, and G. Herranz, ACS Appl. Electron. Mater. **1**, 810 (2019).

[24] A. Rastogi, J.J. Pulikkotil, and R.C. Budhani, Phys. Rev. B - Condens. Matter Mater. Phys. **89**, 1 (2014).

[25] E. Di Gennaro, U. Coscia, G. Ambrosone, A. Khare, F.M. Granozio, and U.S. Di Uccio, Sci. Rep. **5**, 1 (2015).

[26] P.M. Mooney, J. Appl. Phys. **67**, R1 (1990).

[27] Z. Huang, Ariando, X. Renshaw Wang, A. Rusydi, J. Chen, H. Yang, and T. Venkatesan, Adv. Mater. **30**, 1 (2018).

[28] A. Brinkman, M. Huijben, M. Van Zalk, J. Huijben, U. Zeitler, J.C. Maan, W.G. Van Der Wiel, G. Rijnders, D.H.A. Blank, and H. Hilgenkamp, Nat. Mater. **6**, 493 (2007).

[29] C. Cantoni, J. Gazquez, F. Miletto Granozio, M.P. Oxley, M. Varela, A.R. Lupini, S.J. Pennycook, C. Aruta, U.S. Di Uccio, P. Perna, and D. MacCariello, Adv. Mater. **24**, 3952 (2012).

[30] N. Nakagawa, H.Y. Hwang, and D.A. Muller, Nat. Mater. **5**, 204 (2006).

[31] Z.Q. Liu, C.J. Li, W.M. Lü, X.H. Huang, Z. Huang, S.W. Zeng, X.P. Qiu, L.S. Huang, A. Annadi, J.S. Chen, J.M.D. Coey, T. Venkatesan, and Ariando, Phys. Rev. X **3**, 1 (2013).

[32] L. Yu and A. Zunger, Nat. Commun. **5**, 1 (2014).

[33] K. Yoshimatsu, R. Yasuhara, H. Kumigashira, and M. Oshima, Phys. Rev. Lett. **101**, 1 (2008).

[34] O. Copie, V. Garcia, C. Bödefeld, C. Carrétéro, M. Bibes, G. Herranz, E. Jacquet, J.L. Maurice, B. Vinter, S. Fusil, K. Bouzehouane, H. Jaffrès, and A. Barthélémy, Phys. Rev. Lett. **102**, 1 (2009).

[35] F. Gunkel, D. V. Christensen, Y.Z. Chen, and N. Pryds, Appl. Phys. Lett. **116**, (2020).

[36] K. Xiong, J. Robertson, and S.J. Clark, Microelectron. Eng. **85**, 65 (2008).

[37] K. Xiong, J. Robertson, and S.J. Clark, Appl. Phys. Lett. **89**, 5 (2006).

[38] S. Guodong, L. Hui, D. Juanli, Z. Wenxue, Z. Hongyan, and L. Lu, Rare Met. Mater. Eng. **44**, 1099 (2015).

[39] A.K. Ghosh, R.R. Addiss, and R.B. Lauer, J. Appl. Phys. **44**, 3798 (1973).

[40] W. Liu and C.A. Randall, J. Am. Ceram. Soc. **91**, 3245 (2008).

[41] B. Wang, P. Saadatkia, F.A. Selim, and D. Look, J. Electron. Mater. **47**, 604 (2018).

[42] I.I. Piyanzina, V. Eyert, Y. V. Lysogorskiy, D.A. Tayurskii, and T. Kopp, J. Phys. Condens. Matter **31**, 1 (2019).

[43] N. Pavlenko, T. Kopp, E.Y. Tsymbal, J. Mannhart, and G.A. Sawatzky, Phys. Rev. B - Condens. Matter Mater. Phys. **86**, 1 (2012).

[44] N. Palina, A. Annadi, T.C. Asmara, C. Diao, X. Yu, M.B.H. Breese, T. Venkatesan, Ariando, and A. Rusydi, Phys. Chem. Chem. Phys. **18**, 13844 (2016).

[45] N. Osawa, R. Takahashi, and M. Lippmaa, Appl. Phys. Lett. **110**, (2017).

[46] Y. Seo, M. Yeong Song, S. Park, and T. Geun Kim, Appl. Phys. Lett. **100**, 4 (2012).

[47] F.A. Selim, D. Winarski, C.R. Varney, M.C. Tarun, J. Ji, and M.D. McCluskey, Results Phys. **5**, 28 (2015).

[48] T. Tanaka, K. Matsunaga, Y. Ikuhara, and T. Yamamoto, Phys. Rev. B - Condens. Matter Mater. Phys. **68**, 1 (2003).

[49] A. Janotti, J.B. Varley, M. Choi, and C.G. Van De Walle, Phys. Rev. B - Condens. Matter Mater. Phys. **90**, 1 (2014).

[50] D. Manger, B. Kaczer, N. Menou, S. Clima, D.J. Wouters, V. V. Afanas'ev, and J.A. Kittl, Microelectron. Eng. **86**, 1815 (2009).

[51] B. Liu, V.R. Cooper, H. Xu, H. Xiao, Y. Zhang, and W.J. Weber, Phys. Chem. Chem. Phys. **16**, 15590 (2014).

[52] A. Kalabukhov, R. Gunnarsson, J. Börjesson, E. Olsson, T. Claeson, and D. Winkler, Phys. Rev. B - Condens. Matter Mater. Phys. **75**, 2 (2007).

[53] A. Gloter, G. Tieri, D. Li, M. Caputo, V.N. Strocov, O. Stéphan, J.M. Triscone, and S. Gariglio, APL Mater. **8**, (2020).

[54] G. Yuan, C. Li, J. Yin, Z. Liu, D. Wu, and A. Uedono, J. Phys. D. Appl. Phys. **45**, 1 (2012).

[55] D. V. Lang, J. Appl. Phys. **45**, 3023 (1974).

[56] S. Weiss and R. Kassing, Solid State Electron. **31**, 1733 (1988).

[57] S.K. Kim, S.I. Kim, J.H. Hwang, J.S. Kim, and S.H. Baek, Appl. Phys. Lett. **102**, (2013).

[58] S. Wu, G. Wu, J. Qing, X. Zhou, D. Bao, G. Yang, and S. Li, NPG Asia Mater. **5**, e65 (2013).

[59] L. Li, C. Richter, S. Paetel, T. Kopp, J. Mannhart, and R.C. Ashoori, Science (80-.). **332**, 825 (2011).

[60] S. Wu, X. Luo, S. Turner, H. Peng, W. Lin, J. Ding, A. David, B. Wang, G. Van Tendeloo, J. Wang, and T. Wu, Phys. Rev. X **3**, 1 (2014).

[61] C.W. Bark, P. Sharma, Y. Wang, S.H. Baek, S. Lee, S. Ryu, C.M. Folkman, T.R. Paudel, A. Kumar, S. V. Kalinin, A. Sokolov, E.Y. Tsymbal, M.S. Rzchowski, A. Gruverman, and C.B. Eom, Nano Lett. **12**, 1765 (2012).

[62] S.K. Kim, S.I. Kim, H. Lim, D.S. Jeong, B. Kwon, S.H. Baek, and J.S. Kim, Sci. Rep. **5**, 8023 (2015).

[63] R. Pentcheva, M. Huijben, K. Otte, W.E. Pickett, J.E. Kleibeuker, J. Huijben, H. Boschker, D. Kockmann, W. Siemons, G. Koster, H.J.W. Zandvliet, G. Rijnders, D.H.A. Blank, H. Hilgenkamp, and A. Brinkman, Phys. Rev. Lett. **104**, 2 (2010).

[64] A.V.P. Coelho, M.C. Adam, and H. Boudinov, J. Phys. D. Appl. Phys. **44**, 305303 (2011).

[65] K. Yamasaki, M. Yoshida, and T. Sugano, Jpn. J. Appl. Phys. **18**, 113 (1979).

[66] K. Song, T. Min, J. Seo, S. Ryu, H. Lee, Z. Wang, S.Y. Choi, J. Lee, C.B. Eom, and S.H. Oh, Adv. Sci. **8**, 1 (2021).

[67] S. Stemmer and S. James Allen, Annu. Rev. Mater. Res. **44**, 151 (2014).

PLEASE CITE THIS ARTICLE AS DOI: 10.1063/5.0101255

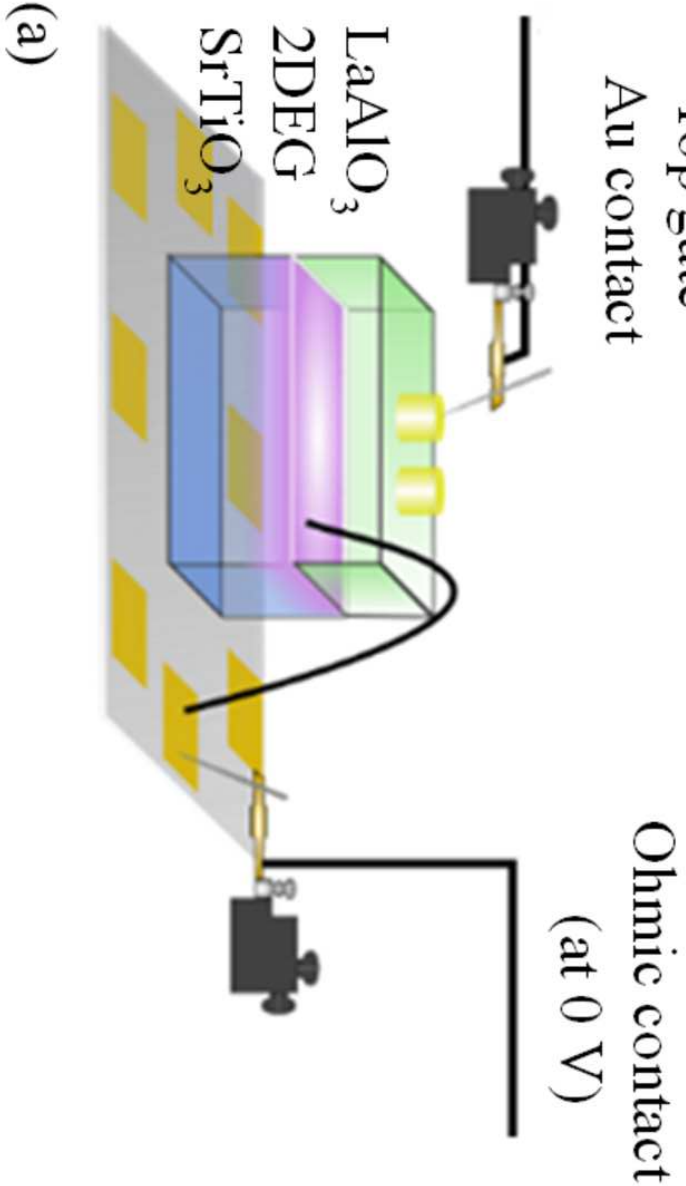

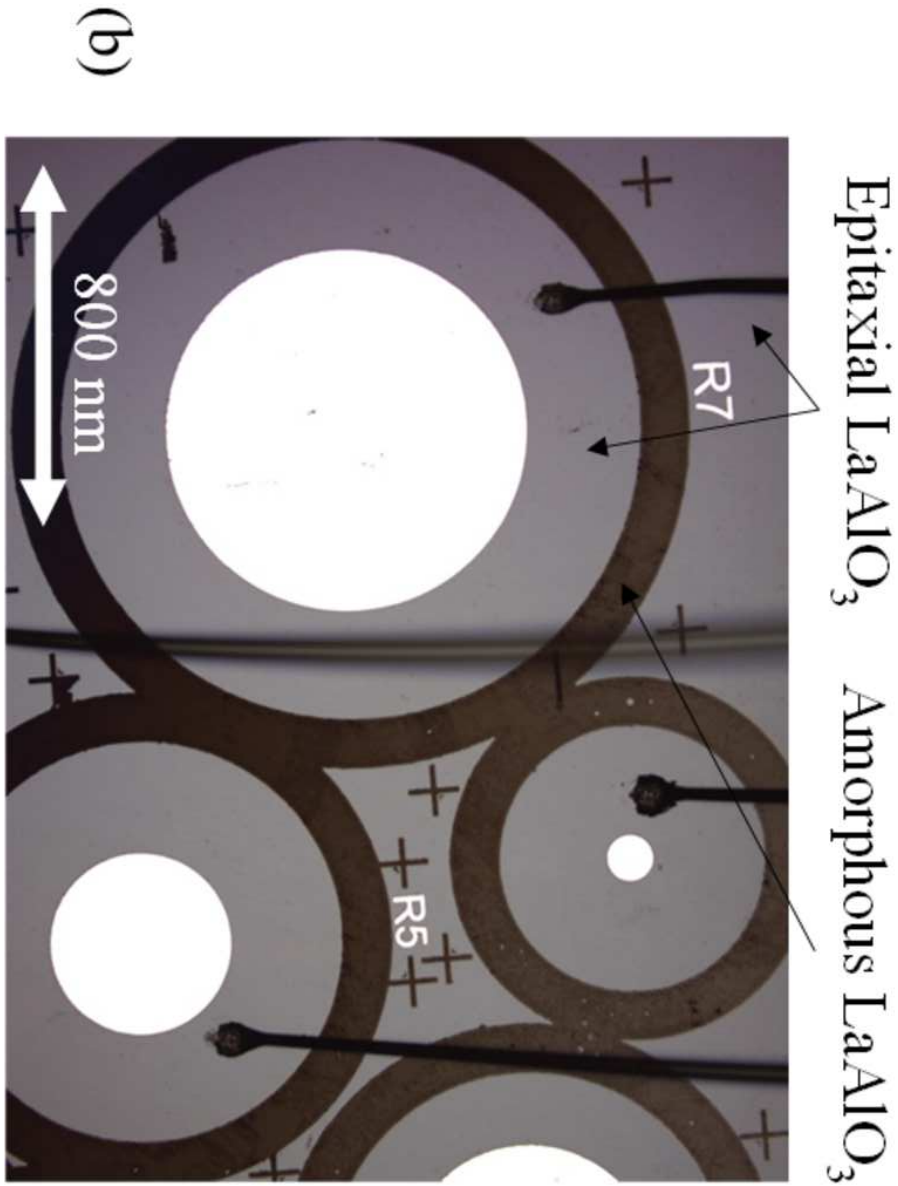

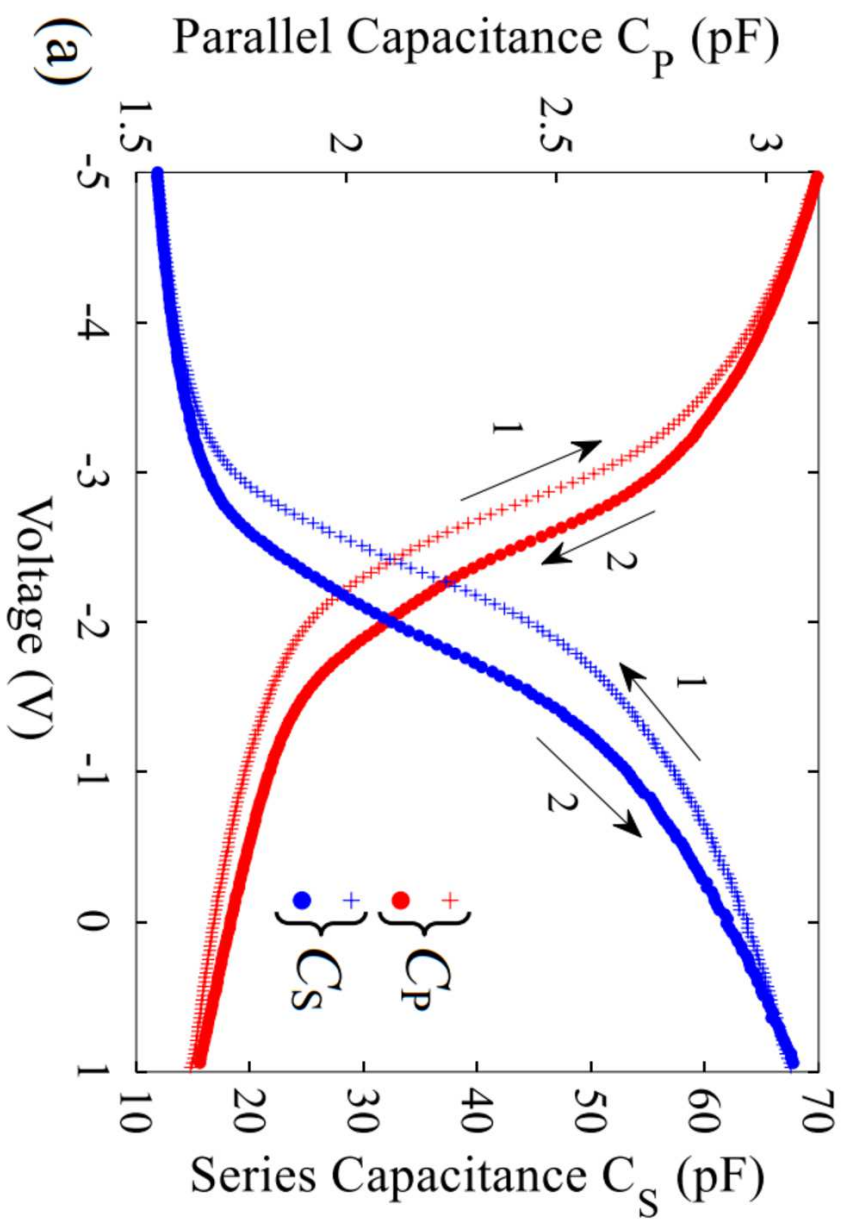

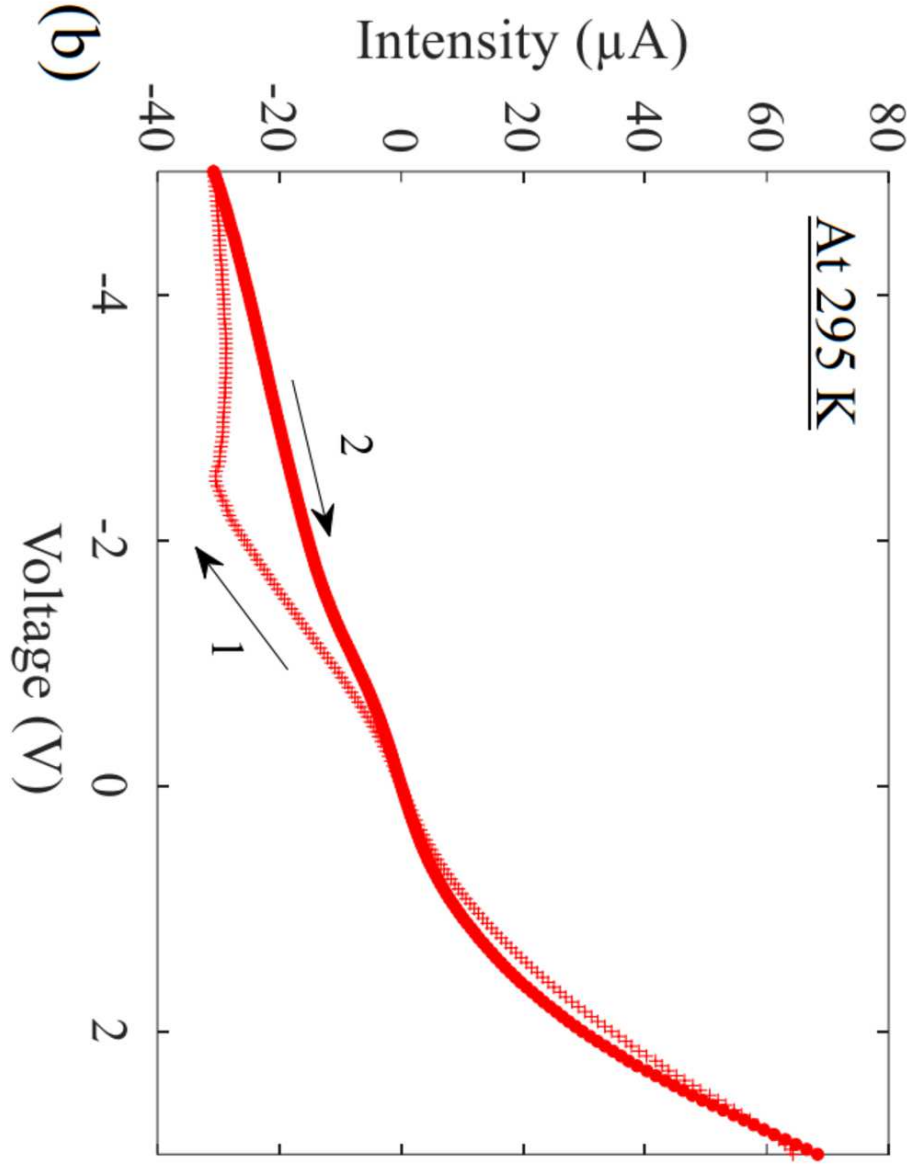

PLEASE CITE THIS ARTICLE AS DOI: 10.1063/5.0101255